Incorporating heat stress treatment into the DO_3SE phenology function for PBW550 wheat (*Triticum aestivum)* cultivar

Adarsh R

MS15036

A dissertation submitted for the partial fulfilment of BS-MS dual degree in Science

Indian Institute of Science Education and Research Mohali

May 2020

Dedicated to all helpless farmers of India

Certificate of Examination

This is to certify that the dissertation titled “Evaluating the impact of different thermal growing conditions and ozone on PBW550 wheat (Triticum Aestivum) cultivar” submitted by Mr. Adarsh R (Reg. No. MS15036) for the partial fulfilment of BS-MS dual degree programme of the Institute, has been examined by the thesis committee duly appointed by the Institute. The committee finds the work done by the candidate satisfactory and recommends that the report be accepted.

Dr. Baerbel. Sinha (Supervisor)

Dr. Anoop Ambili

Dr. Raju Attada

Dated: 4, May, 2020

Declaration

The work presented in this dissertation has been carried out by me under the guidance of Dr. Baerbel Sinha at the Indian Institute of Science Education and Research Mohali.
This work has not been submitted in part or in full for a degree, a diploma, or a fellowship to any other university or institute. Whenever contributions of others are involved, every effort is made to indicate this clearly, with due acknowledgement of collaborative research and discussions. This thesis is a bonafide record of original work done by me and all sources listed within have been detailed in the bibliography.

Adarsh R
(Candidate)

Dated: 4-5-2020

In my capacity as the supervisor of the candidate's project work, I certify that the above statements by the candidate are true to the best of my knowledge.

Dr. Baerbel Sinha
(Supervisor)

Acknowledgments

I sincerely thank my supervisor, Dr. Baerbel Sinha, for her constant support, patient teachings and timely inputs. I take this opportunity to thank Dr. Vinayak Sinha for exposing me to different disciplines of Environmental Science and providing useful inputs. I also thank my thesis committee members Dr. Raju Attada and Dr. Anoop Ambili for their valuable time and for supporting me throughout.

I'm grateful to all my lab mates for maintaining a cheerful lab environment. Special thanks to Abhishek, Harshita and Savita for guiding me through the course of my thesis project.

Thanks to my buddies Madhuvanthi, Leesa, Swastik, Vivek and Puneeth for making my life at IISER Mohali fun-filled and memorable.

Finally, I thank my parents, Latha and Raghuram, my brother, Harsha, and my sister, Ramya, for their unconditional love and constant support.

List of Figures

List of Tables

Notation (abbreviations)

O_3	Tropospheric ozone
CO_2	Carbon dioxide
IGP	Indo-gangetic Plain
g_{sto}	Stomatal conductance
SM	Soil moisture.
VPD	Vapour pressure deficit
DAS	Days after sowing
DAA	Days after anthesis
AOT40	Accumulated Ozone exposure over the threshold of 40 ppb
M7	Average 7-hour ozone concentration, between 09:00 and 16:00 hours

.

CONTENTS

Abstract

Modelling of leaf-level stomatal conductance (g_{sto}) with the help of observed or modelled meteorological parameters and environmental response functions has been introduced as a new way to conduct ozone (O_3) damage to vegetation and calculate *triticum aestivum* yield loss based on the absorbed O_3 phytotoxic dose (POD) but has not been used in India so far.

With the help of environmental response functions and the yield data of relay seeding experiments for the *triticum aestivum* cultivar PBW550 we explore the impact of meteorological parameters and ozone stress on wheat yields. The cultivar was directly obtained from breeders and was sown on 1st and 15th November as well as on 1st December in 2018. Harvest occurred in April 2018 and April 2019, respectively.

We subsequently use meteorological observations and ozone measurements obtained at the Central Atmospheric Chemistry facility of IISER Mohali in Punjab, India phenology observations and a large number of yield related parameters to estimate how adverse meteorological conditions and ozone exposure during different growth stages of the plant impact plant growth and yield. To this end we parametrise the DO_3SE model for PB550 with the help of stomatal conductance measurements during the growing season. We also develop an improved phenology function which allows incorporation of the effects of heat stress on leaf phenology into the DO_3SE model in a manner which is consistent with the treatment of the heat stress in crop models.

We find, that contrary to the present practice in the ozone-crop yield loss community, wheat yield is not only affected by environmental stress and ozone exposure during the flowering and grain filling stage of the plant, but also when the growth phase changes from vegetative to reproductive (tillering to heading). This stage is equally important for the final yield as the number of active tillers per plant and the length of the head is determined during these growth stages. Unlike flowering and grain filling this developmental period is rarely affected by heat stress, making ozone the most important stressor affecting plant growth during this crucial phase. In the light of these findings we revisit the ozone accumulation window currently recommended for assessing ozone related crop yield losses in *Triticum aestivum*.

Chapter 1

Introduction

Cultivated over an area of 215 million hectares annually, Wheat (*Triticum aestivum*) is the most widely produced commercial crop in the world, currently consumed by 215 million people spread across 89 countries. (CGIAR : https://wheat.org/wheat-in-the-world/). Different cultivars of wheat exist, which are adapted to different agro-climatic conditions, making it a versatile crop. In the major wheat producing nations of the world, winter wheat cultivars - strains of wheat sown at the onset of winter and harvested during late spring - are the most widely cultivated variety (Asseng, Foster, and Turner 2011). In India, the second largest contributor to global wheat production (FAO, 2018), Punjab, known as the bread basket of India, has been the top contributor and put together with Haryana, they produced nearly 50% of India's wheat procured and redistributed by the Department of Food and Public Distribution in the year 2017-18 (Agricultural Statistics, 2017 : http://agricoop.nic.in/sites/default/files/pocketbook_0.pdf). Wheat being a rabi crop in India, farmers of Punjab and Haryana cultivate a spring wheat cultivars or hybridizations of spring and winter wheat which are sown in November and harvested in March/April (Chnneja et al., 2015; Joshi et al., 2003; Ortinez, Dhillon, Fischer, 1994)

While many studies have reported that the crop growth is controlled by various abiotic and biotic factors including temperature, solar radiation and rainfall, a smaller number of them report the impact of agro-climatic extremes on crop yield**.** In order to explore these relationships, good understanding of growth stages of wheat is crucial.

1.1 Growth and development of wheat:

Wheat cultivars are broadly classified as winter wheat and spring wheat, on the basis of response to vernalization (See section 1.2). Once sown, it takes anywhere between 140-

170 days for wheat to reach maturity, depending on the cultivar, sowing date and management practices. A total of 5 major phases of development are observed between sowing and maturity, which are described in Table 1. Wheat growth is often expressed in one of the cereal growth staging scales - Feekes scale, Zadoks scale or BBCH – scale.

The growth of wheat is divided into 2 phases – vegetative growth phase and reproductive growth phase. During vegetative growth, the first growth phase, most of the photosynthetic produce is utilised in the development of vegetative organs (not involved in reproduction) – roots, leaves and stem. The reproductive growth primarily involves the development of flowers, the reproductive organ in plants. Flowering marks the end of plant growth and development, for all the processed and stored products of photosynthesis are translocated to the fertilized ova (grain), through a process called grain filling. The sub-stages of vegetative and reproductive phases are explained in sections starting from 1.1.1.

Table 1: Phases of development in wheat

Stage code	Description	Plant parts growing	Duration (in ◦C-days)
1	Sowing to emergence	Roots, coleoptile	-
2	Emergence to Flag leaf	Root, stem, leaves	1000 - 1100
3	Flag leaf to Heading	Root, stem, leaves	150 - 200
4	Heading to Anthesis	Root, stem, leaves, ear	100 - 200
5	Anthesis to Maturity	Root, stem, grain	1000 - 1200

The major factors that control wheat growth and development are temperature, solar radiation, water availability and nutrient availability. Since the last two are under the control of the farmer in the case of irrigated farmlands, the development is controlled by temperature and solar radiation (See Section 1.2). Note that the duration between the developmental stages of wheat is expressed in thermal time (TT) in the units of ℃ days (Eq. 1), as it has been observed that plants need to be exposed to certain amounts of heat

in order to grow from one developmental stage to the next. Using calendar days instead of TT does not account for the interannual variations in weather conditions, and is therefore less accurate.

$$TT = \begin{cases} \Sigma\, \Delta TT * \min(f_v\,, f_p) & For\ stages\ 1\ and\ 2 \\ \Sigma\, \Delta TT & For\ stages\ 3\ and\ above \end{cases} \quad \text{(Eq. 1)}$$

where f_v is the vernalization factor and f_p is the photoperiod factor

Although the crop modelling community conventionally uses thermal time to refer to the duration of plant growth and development, the definition of thermal time itself differs between crop simulation models (Jones et al., 2003; Zheng et al., 2014). In simple, thermal time can be defined as the summation of daily thermal time (ΔTT), which is the daily temperature accumulation, expressed in the units of ℃ days, in the absence of snow (Eq.2).

$$\Delta TT = \begin{cases} T_{avg} & 0 < T_{avg} \leq 26 \\ \frac{26}{8}(34 - T_{avg}) & 26 < T_{avg} \leq 34 \\ 0 & T_{avg} < 0 \ or \ T_{avg} > 34 \end{cases} \quad \text{(Eq. 2)}$$

ΔTT is a function of T_{avg}, the average of daily maximum and daily minimum temperatures. The factors involved in the calculation of ΔTT and TT are explained in Section 1.2. While this study deals only with winter wheat cultivars grown in the absence of snow, the documentation of APSIM-Wheat module and DSSAT-Wheat model (Zheng et al., 2014; Jones et al,. 2003) contain detailed explanation of the same, for other cases.

1.1.1 Sowing to emergence (Stage 1)

The seeds germinate after sowing, resulting in development of primary root (radical) and primary shoot (plumule). Further, leaf primordia are developed (covered by a protective structure named coleoptile) which eventually grow into leaves. Emergence is marked by the appearance of the main shoot over the soil surface. From the date of sowing,

emergence takes between 2 and 7 days for Indian winter wheat, depending on the cultivar and sowing date.

1.1.2 Emergence to Flag leaf (Stage 2)

Vegetative growth picks up pace after emergence. An important phase of development after emergence is the development of tillers – lateral branches that originate at the coleoptilar node, sharing root mass with the primary shoot (stem). Each tiller bears a spike or head (structures housing wheat grains) and therefore the number of tillers developed, which depends on various factors including sowing date and nutrient availability, is important in deciding the yield (Kirby E.J.M, 2002).

The growth of primary stem and tillers is accompanied by development of leaves and secondary roots. As the shoots grow erect out of the soil surface, tillering ends and more number of nodes (points on the shoot where leaves or buds originate, characterised by swollen areas with darker shade of green than the rest of the shoot) are visible. Development of leaves on the main stem and tillers progresses in an identical fashion; flag leaf, the last leaf to develop, appears at the tip of the shoot, any time between 65-95 days after sowing (DAS) for Indian winter wheat, depending on the cultivar and sowing date. A healthy flag leaf makes 48% contribution to grain yield (El Wazziki et al., 2015), the largest of all photosynthetically active plant parts. The completion of flag leaf growth marks the end of vegetative growth phase; beyond this stage, all photosynthetic produce is stored in different plant parts and are translocated to grains, after fertilization.

1.1.3 Flag leaf to Heading (Stage 3)

Heading is the first stage of reproductive growth phase, where the development of the apex of the stem called head or spike begins. The morphological stages of development include the double ridge stage, which changes the shoot apex growth phase from vegetative to reproductive (Acevedo E, 2002 and Kirby E.J.M, 2002). After the flag leaf develops completely, wheat enters a developmental stage called booting, where the head or spike – flower bearing plant part – is formed and covered in leaf sheath below the flag leaf. The heads grow erect out of the flag leaf ligule (base of the flag leaf) between 73 and 101 DAS for Indian winter wheat, depending on the cultivar and sowing date.

1.1.4 Heading to Anthesis (Stage 4)

Initiation of anthesis or flowering occurs between 92 and 115 DAS for Indian winter wheat, depending on the cultivar and sowing date. Majority of the florets are self-pollinated, starting with the central portion of the spike and extending towards either ends (Acevedo E, 2002). The entire process which results in the formation of wheat grains lasts 3 to 10 days, depending on the climate and cultivar (Kirby E.J.M, 2002). An important physiological change that begins at this stage is leaf senescence, which continues until the end of the phenology cycle.

1.1.5 Anthesis to Maturity (Stage 5)

Successful fertilization in florets leads to development of zygote and endosperm, which together make up the wheat grain. The following process is called grain filling, where the starch stored in various plant parts is translocated to the grain. Upon completion of anthesis, the rate of leaf senescence increases and the plant begins to turn yellow. When most of the plant turns yellow and the wheat kernels are hard, wheat reaches maturity and is ready to be harvested.

1.2 Temperature control of wheat growth

The most important climate factor that controls wheat growth is temperature. The base temperature for wheat below which no growth is observed is reported to be 0°C in some cases while some have reported 4°C (Cao and Moss, 1989). According to the crop modelling community, the optimum temperature range for photosynthesis and hence for growth, is between 12°C and 26°C, and the rate of photosynthesis decreases beyond that, dropping to zero after 34°C (Zheng et al., 2014). However, the optimum and the maximum temperatures are different for different cultivars, which can be calculated experimentally using stomatal conductance measurements. Equation 2 (Eq. 2) describes the effect of temperature range on calculation of ΔTT.

Completion of each of the growth phases is marked by accumulation of a certain amount of temperature, as described in Table 1. However, the calculation of TT is not the same

for all growth stages, as described by equation 1 (Eq. 1). Growth stages 1 and 2, which fall under vegetative growth phase, are limited the vernalization factor f_v and the photoperiod factor f_p. Winter wheat does not proceed into the reproductive growth phase, unless it is exposed to certain duration of cold temperatures, a process called vernalization; f_v is related to vernalization and an experimentally determined constant of sensitivity to vernalization (Winter wheat varieties are more sensitive to vernalization while spring wheat varieties are less so). The vegetative growth phase for winter wheat is extended if vernalization requirements are not met, resulting in delayed flowering. Spring wheat does not require vernalisation but can be photosensitive. Most spring wheat cultivars can be sown year around and require neither vernalization nor increasing daylength to enter into reproductive growth. The factor f_p accounts for photoperiod or day length. The forms of both f_v and f_p are complex and can be obtained from APSIM Wheat documentation (Zheng et al, 2014).

1.3 Factors limiting wheat growth

Temperature, solar radiation, water and nutrient availability are the factors that control wheat growth. Stress in the form of any one of these factors can affect the phenology, resulting is reduction of yield. While stress can be both in excess or deficit of required amounts, within the scientific community the definition of stress is often different for different factors; for water and nutrient availability, stress refers to deficit of required amounts and for temperature (heat), stress refers to excess of required amounts. Multiple studies have explored the detrimental effects of heat (temperature) stress and water stress (Viswanathan and Chopra, 2001; Asseng et al., 2015; Iqbal et al., 2017) while fewer have examined the impacts of nutrient stress. The major wheat producing belt in India lies in the North western IGP, where most of the area under cultivation is irrigated. Hence the major stress faced by crops is due to heat.

Another major source of stress for many plants, including wheat, is tropospheric ozone, which affects the growth in many ways. Upon entering the leaves through stomata, ozone generates reactive oxygen species, hampering the metabolism and leading to destruction of cell membrane (Zhao et al., 2007). Cumulative growing season ozone stress has been observed to cause effects such as premature aging of leaves (early senescence), reduced flower number, reduction in yield and so on (CLRTAP, 2015).

Tropospheric O_3 is measured using two exposure based metrics, AOT40 and M7. AOT40 is defined as the summation of difference between hourly average ozone concentration and a threshold value of 40 ppb and M7 is the –hour average ozone concentration measured between 09:00 hours and 16:00 hours.

The results from studies examining the impacts of heat stress and tropospheric ozone stress on wheat is reviewed in the next chapter.

Chapter 2

Review of Literature

Wheat production in India is severely affected by 2 major agro-climatic stress factors: heat and tropospheric ozone. They directly impact the phenology, which ultimately results in reduction of yield. The following sections describe the qualitative and quantitative impacts of heat and ozone stress on wheat, as reported by previously conducted studies.

2.1 Impact of heat stress on wheat growth and development

Wheat has a natural temperature threshold greater than the optimum temperature for photosynthesis, until whichen there is no negative effect of heat (high temperature) on growth and development. Increase in temperature beyond this threshold for a sufficient period is called heat stress, which induces irreversible damage to plant growth and development (Hall, 2000). The impact of heat stress on wheat has been studied through both, field experiments and model simulations. However, the incorporation of heat stress into crop simulation models has only been a recent advancement (Asseng et al., 2011; Barlow et al., 2015).

Multiple experimental studies performed under field and controlled conditions have shown that heat stress affects wheat morphology, physiology and biochemistry (Iqbal et al., 2017). A review on wheat growth and development response to temperature at different growth stages by Porter et al., (1999) identified the lethal temperature (maximum) for wheat as 47.5°C. The study also lists the minimum, optimum and maximum temperatures and the corresponding growth rates, for different developmental stages of wheat. As mentioned in Section 1.2 of Chapter 1, reproductive growth for

winter wheat is not initiated without fulfilment of vernalization requirements. Through his study on temperature effects on vernalization, Brooking (1996) showed that during vegetative growth phase, temperatures greater than 11°C reduce the rate of vernalization while those above 18°C halt the process altogether. However, under field conditions, the chances of winter wheat experiencing heat stress, is significantly greater around the anthesis stage, which begins post-heading. While it is normal for photosynthesis rate of flag leaves to decline after anthesis, high temperatures accelerate the decrease, shortening the grain filling duration, resulting in reduced grain mass (Shah et al., 2003). In India, most cultivars commonly grown as "winter wheat" are, genetically speaking, spring wheat cultivars which have no vernalisation requirement and flower when a day length of 12 hours and an average temperature of 25°C is attained (Kumar et al., 2012). In the Indian context, Viswanathan et al., (2001) showed that for winter wheat cultivars suitable for normal and late sowing in the North Indian plains, heat stress accelerates grain filling rate, but reduces grain filling duration, resulting in reduced grain weight. The study further reported that heat stress inhibits synthesis of starch and proteins. In a study conducted with 108 wheat cultivars under controlled conditions, Qaseem et al., (2019) reported that exposure to heat stress reduced 53.05% of grain yield and caused disintegration of chlorophyll and proteins. Heat stress hastens leaf senescence leading to reduction in leaf area, which directly affects the photosynthesis rate (Shah et al., 2003). The biochemical basis of hastened leaf senescence and reduced grain weight due to heat stress was examined by Zhao et al., (2007). For the Indo-Gangetic plain (IGP), Lobell et al., (2012) conducted a study using MODIS satellite data, which concluded that an average increase of 2°C in IGP would result in shortening of photosynthetically active duration of wheat growing season by 9 days, due to accelerated leaf senescence.

Most crop simulation models (CSM) do not incorporate crop responses to elevated temperatures (Rötter et al., 2011). Although some CSMs have reproduced the observed impacts of heat stress on wheat, the uncertainties involved in modelling such effects make the estimates less accurate (Asseng et al., 2013). Rather than any single model, median of multi-model ensembles for crop response at elevated temperatures has been shown to be more accurate (Asseng et al., 2014; Martre et al., 2015). A comparison of responses of 4 popular crop models to heat stress at anthesis and grain filling was performed by Liu et al., (2016), which examined the uncertainties in reduction of grain filling duration, grain weight and visible leaf area for all models. A simulation study performed by Dubey et al.,

(2020) using projected climate scenario, predicted that terminal heat stress on wheat will result in 16% and 11.1% reduction in yield for years 2020 and 2050 respectively, for Indian region.

2.2 Impact of Tropospheric ozone on wheat growth and development

Tropospheric ozone (O_3), a greenhouse gas present in large concentrations over agricultural regions, is one of the most harmful pollutants for vegetation, due to its phytotoxic nature (Ainsworth et al., 2012). Apart from causing damage to cell membrane and disrupting the metabolism of photosynthesis, O_3 is known to induce leaf damage, premature aging of leaves, reduced flower numbers and reduced yield quality and quantity (CLRTAP, 2015). Global percentage yield loss in wheat due to O_3 is estimated to be 13.8%, 13.4% and 9.4% for AOT40, M7 and POD3IAM metrics respectively, with loss over Indian region being high at 25%, 21.5 and 12.2% for the same metrics (Mills et al., 2018). The relative yield loss over Punjab and Haryana, the top two states contributing to India's wheat, was estimated to be 27-41%, based on AOT40 metric (B. Sinha et al., 2015). However, the stomatal flux of O_3 has been observed to be more strongly impacting the observed effects O_3 vegetation, than the concentration of O_3 around plants (Mills et al., 2011).

Simulating stomatal flux of ozone through modelling studies had played an important role in estimating yield loss due to exposure to O_3, based on stomatal-flux based critical level metrics for O_3. One such model extensively used to study the effects of O_3 on vegetation in the European countries is the DO_3SE (Deposition of Ozone and Stomatal Exchange), which has been parameterised for European wheat cultivars (Pleijel et al., 2007; CLRTAP, 2015).

The DO_3SE model has not been parametrised for Indian region. The phenology function which is a part of the model, does not take into consideration the impact of heat stress on hastening leaf senescence while on the other hand, crop simulation models do not account for O_3 effects on leaf senescence. Through this study, we parametrise the DO_3SE model

for an Indian winter wheat cultivar (PBW550) with the help of stomatal conductance measurements. We also develop an improved phenology function which allows the incorporation of the effects of heat stress on leaf phenology into the DO_3SE model in a manner which is consistent with the treatment of the heat stress in crop models.

Chapter 3

Materials and Methods

3.1 Site description

This study was carried out at IISER Mohali (30˚39’51.54 N 76˚43’55.65 E), SAS Nagar, Punjab, India (figure 1). Located in the North-Western IGP, Punjab has a subtropical winter dry steppe climate, which combined with fertile alluvial soil rich in nutrients, makes the condition suitable for winter wheat cultivation. For this study, wheat was cultivated on a plot of land, within the IISER Mohali campus, between November 2018 and April 2019.

Figure 1 : Location of IISER Mohai (Blue pin), wheat field within IISER Mohali campus (Yellow pin) and Air quality station (Red pin), marked on Google Earth image.

3.2 Agricultural methodologies – Wheat cultivation

The winter wheat cultivar used for this study is PBW550. This is a superior cultivar suited for late sowing in irrigated croplands, popular in the NW-IGP. It was developed in Punjab Agricultural University, Punjab, India, in 2007 and is known for good grain quality and early maturity. It is resistant to pest and most fungal infections. It is resistant to thermal heat stress and has a maturity time of 146 days.

The methods involved in preparing the plot before sowing included tilling (top layer only), harrowing and levelling. Rotavator was used for uniform mixing and breaking down blocks of soil. Pre-sowing irrigation was applied and weeds were pulled out manually. When the right moisture level was reached, the field was ploughed using harrow, after which, organic manure was applied and rotavator was used to mix the applied manure uniformly. A total of 3 plots were prepared for sowing on 3 different dates - 1st November 2018 (Plot 1), 15th November 2018 (Plot 2) and 1st December 2018 (Plot 3). A metallic rod was used to make holes of depth close to 2 inches into which wheat seeds were sown manually. 2 seeds were sown in each hole and after emergence the smaller of the two plants was removed manually.

A total of 10 winter wheat cultivars were sown in each plot, which contained 3 rows. Each row contained 30 plants of each cultivar, with spacing being plants 23 cm between intra-cultivar and 44 cm between inter-cultivar plants.

Soil moisture was maintained at healthy levels throughout the growing season and the plots were irrigated as and when required. 40 Kg of urea was used per acre, which was applied during the flag leaf stage, although no other chemical fertilizer or pesticide was used. Weeding was performed manually for once in ten days.

Plot 1 was harvested on 10th April 2019, plot 2 was harvested on 14th April 2019 and plot 3 was harvested on 18th April 2019.

3.3 Collection and processing of Wheat Phenology data

The number of plants at one growth stage was counted manually on alternate days, for all plots and all growth stages – emergence, flag leaf, heading and anthesis. The fraction of plants reaching a particular growth stage was plotted against days after sowing (DAS) and sigmoid growth curve was used for fitting the resulting scatter points. For a given plot and a particular growth stage, DAS at which half of the total number of plants reached the growth stage was calculated from the curve, which was assigned as DAS for that plot and that growth stage. The plots for flag leaf, heading and anthesis stage for all plots is shown in figure 2. The X_{half} parameter of the sigmoid function gives the DAS count at which 50% of the plants have emerged or reached a particular stage.

3.4 Collection and processing of meteorology data

A field meteorology station by decagon (EM50G) was used for measuring temperature and PAR, while wind speed and RH was measured using Met One sensors. Rainfall was measured using a tipping bucket arrangement and tropospheric O_3 was measured with Thermo Fisher Scientific 49i Ozone Analyser. Specifications of all the involved instruments in given below:

(a) **Temperature sensor**: VP-4 temperature sensor was used to record the temperature, which has a working range of -40°C to 80°C. The accuracy is 0.5^{o}C for temperature range of 5^{o}C to 40°C and 1°C for temperatures out of this range.

(b) **PAR and PYR sensor**: QSO-S PAR Photon Flux Sensor was used to record the PAR within the spectral range of 400-700nm with the accuracy of ±5% and PYR solar radiation sensor was used to measure solar radiation within the spectral range of 380-1120 nm with the accuracy of ±5%.

(c) **RH sensor**: A thin film polymer capacitor sensor (Met One 083e) was used to measure the measures the RH with the accuracy of ±2% from 0-100% humidity.

(d) **Wind Speed sensor**: Met One 010C sensor was used to document wind speed with the accuracy of ±1% and the resolution of <0.1 m/s.

(e) **Rain Gauge**: A tipping bucket rain gauge was used for measuring rainfall, which resets after 25mm.

(f) **Ozone Analyser**: A UV photometry based analyser (Thermo Fisher Scientific Model 49i) was used to measure the ozone concentration with the time resolution of 1 minute. The uncertainty of the instrument is <6% and with the detection limit 1 nmol mol^{1}. Zero calibration was performed once every week and span calibrations were performed once every month, with 5 calibration points between 0 and 125 ppb.

All data collected had a temporal resolution of 1 minute. Missing data points were replaced by data available for the missing period from the most recent years of past. Hourly and daily averages were calculated for all meteorological parameters except for rainfall. M7 and AOT40 values were calculated for Ozone using the hourly data.

3.5 Measuring stomatal conductance

Stomatal conductance is the measure of flux of CO_2 or water vapour through stomata of a leaf. For this study, a leaf porometer manufactured by Decagon Devices was used to measure stomatal conductance of water vapour in wheat. Leaf porometer determines the flux of water vapour moving out a leaf by putting the leaf in series with two RH sensors of known conductance, in a diffusion cell. The RH at the end point of the cell is kept at 10% with the help of an anhydrite dryer. The gradient in RH between the saturated air inside leaf's stomata and the dry air at the end of the diffusion chamber triggers the movement of water vapour from inside of the leaf through stomata, which given the total conductance of the system. Subtracting the known conductance between the RH sensors from the total conductance gives the stomatal conductance. A plastic bead is used as an agitator which helps in the mixing of the air and water vapour inside the cell, to flush out any existing water vapour after taking a measurement.

Starting from the flag leaf stage, stomatal conductance measurements were made everyday for all plots between 11:00 hours and 15:00 hours, where a plant from each row of each plot was chosen at random and the stomatal conductance of flag leaf was measured. Since leaf porometer is highly sensitive to moisture, no measurements were made on rainy days and on days when due formation on leaves was observed at the time of making measurement.

3.5.1 Calibrations

Leaf porometer was frequently calibrated manually using moistened filter paper. USP water was used to wet filter paper, just enough to reach 100% RH. The moistened filter paper was then placed on a plastic calibration plate with known conductance of 240 mmol m^{-2} s^{-1}. The measured conductance of the calibration plate was used to calculate the calibration factor as follows:

$$\text{Calibration factor} = \frac{Measured\ conductance\ of\ calibration\ plate}{240\ mmol\ m^{-2}s^{-1}}$$

Wheat stomatal conductance measurements performed after calibration were multiplied with the calibration factor calculated using the above relation.

3.5.2 Ozone stomatal conductance

Leaf porometer measures the stomatal conductance of water vapour. Using Graham's law of diffusion, the diffusion coefficient of ozone with respect to water is 0.663. Therefore the stomatal conductance corrected with calibration factors were multiplied with 0.663 to obtain O_3 stomatal conductance.

3.6 Modelling O_3 stomatal conductance

In the DO_3SE model, O_3 stomatal conductance is modelled using multiplicative algorithm proposed by Jarvis P.G (1976) and modified by Emberson et.al (2000). The existing version of the model was included in the Mapping manual of the (CLRTAP, 2015). The following is the form of the model used to predict O_3 stomatal conductance:

$$g_{sto} = g_{max} * \min\{(f_{phen}, f_{O3})\} * f_{light} * \max\{f_{min}, (f_{temp} * f_{VPD} * f_{SW})\}$$

Where, g_{sto} is the stomatal conductance (mmmlO_3 .93 612.22 Tm[<0003>] TJETBT1345.19 200.06 Tm[

reaches VPD_{min}, the stomatal conductance is minimum and VPD is most limiting.

- f_{SW} is the limitation to stomatal conductance by soil water potential. This factor was not considered for this study, since soil moisture was maintained at healthy levels throughout the growing season.

The fit parameters for all functions are calculated by plotting measured stomatal conductance with each of the parameters and then the maximum curve is fit using the boundary line technique (Jarvis, 1976), which is based on the hypothesises that the curve joining the outermost points encompassing most of data points, represents maximum possible stomatal conductance, for a given value of the parameter.

3.7 Modelling response of stomatal conductance to heat stress

The result from Asseng et al., (2011) - modelling response of relative leaf area index to post-anthesis heat stress using a multiplicative factor F_{heat} to account for accelerated leaf senescence due to heat stress - was reproduced and modified for modelling stomatal conductance response to heat stress. The factor F_{heat} is calculated as follows:

$$F_{heat} = \begin{cases} 1 & for\ T_{max} \leq 34^{o}C \\ 4 - \left(1 - \frac{T_{max} - 34}{2}\right) & for\ T_{max} > 34^{o}C \end{cases}$$

where T_{max} is the daily maximum temperature. F_{heat} is greater than 1 only when there is heat stress, that is, when daily maximum temperature is greater than $34^{o}C$.

Since stomatal conductance is dependent on leaf area, change in stomatal conductance for days after anthesis (DAA) follows the simulated behaviour in relative leaf area index change after anthesis (decreases with DAA). Hence relative leaf area index was replaced by stomatal conductance. The control case simulation of stomatal conductance with 'no heat stress after anthesis' was plotted. Using measured temperature data, days with heat stress events for different wheat plots were identified. For a given plot, if heat stress was first observed on X^{th} DAA, F_{heat} was calculated using T_{max} for that day. The control

simulation sequence of stomatal conductance was labelled NHS (no heat stress). The difference between stomatal conductance from NHS on $(X-1)^{th}$ DAA and X^{th} DAA was multiplied by F_{heat}. This multiplied difference was subtracted from $(X-1)^{th}$ DAA stomatal conductance from NHS and assigned as stomatal conductance for X^{th} DAA of the first heat stress sequence (HS_1). The difference between stomatal conductance of X^{th} and $(X+1)^{th}$ DAA and for other remaining consecutive days from NHS sequence was maintained in HS_1 sequence. In other words, heat stress observed on a given day, accelerated the decrease in stomatal conductance for that day only. If heat stress was observed for more than one day, say the second heat stress event was observed on Y^{th} DAA for a given plot, similar method was followed to generate a second heat stress sequence (HS_2). The difference was that for HS_2, HS_1 was used to calculate the difference in stomatal conductance, instead of NHS. In general, for generating a HS_n sequence (n>1), HS_n-1 sequence of stomatal conductance was used to calculate difference in stomatal conductance.

Chapter 4

Results and Discussion

4.1. Meteorological conditions during the growing season

4.1.1 Temperature

A time series of growing season temperature is shown in figure 2. Starting from the date of sowing for plot 1 (1st November 2018), temperature shows a decreasing trend until January, after which there is no trend observed until the beginning of summer. There is an increasing trend starting from 3rd March, which is observed all the way until the harvest date for plot 3 (18th April 2019).

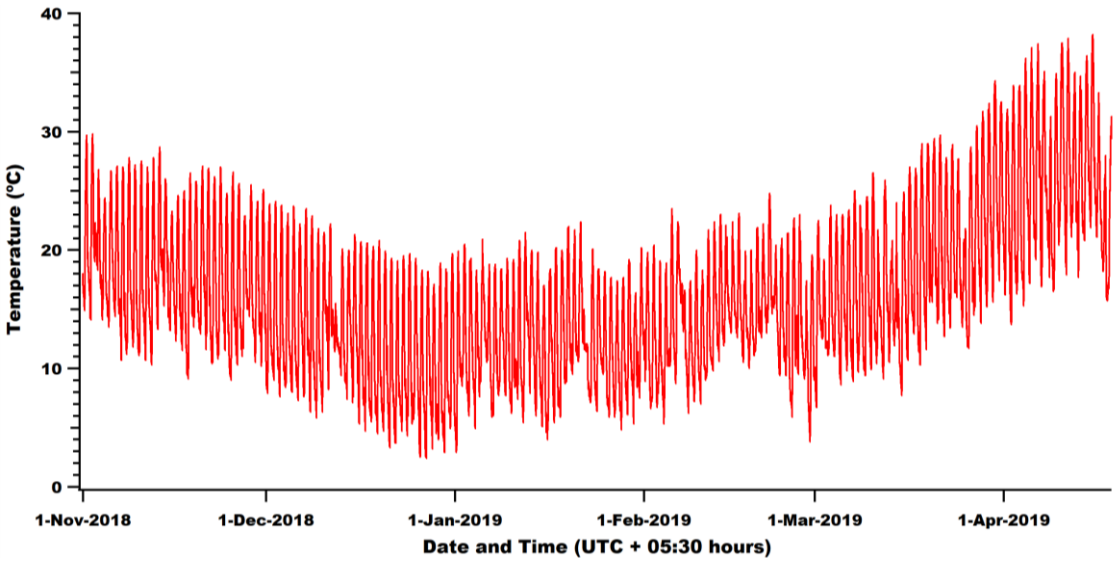

Figure 2: A time series of temperature observed at the Central Atmospheric Chemistry Facility, IISER Mohali, Punjab, India, during 2018-19 winter and early summer of 2019

A maximum temperature of 38.2°C was recorded at 13:38 hours on 15thApril 2019 and a minimum temperature of 2.4°C was recorded at 07:33 hours on 27th December 2018.

Although there were heat stress events (temperature greater than 34^{o}C), the temperature did not reach lethal values (Porter et.al, 1999) during the growing season.

The daily average temperature is plotted along with daily minimum and daily maximum temperatures in figure 3. The trends in daily average temperature during the growing season are apparent from the plot, where the trends in daily minimum and daily maximum temperatures are in agreement with that of daily average temperature.

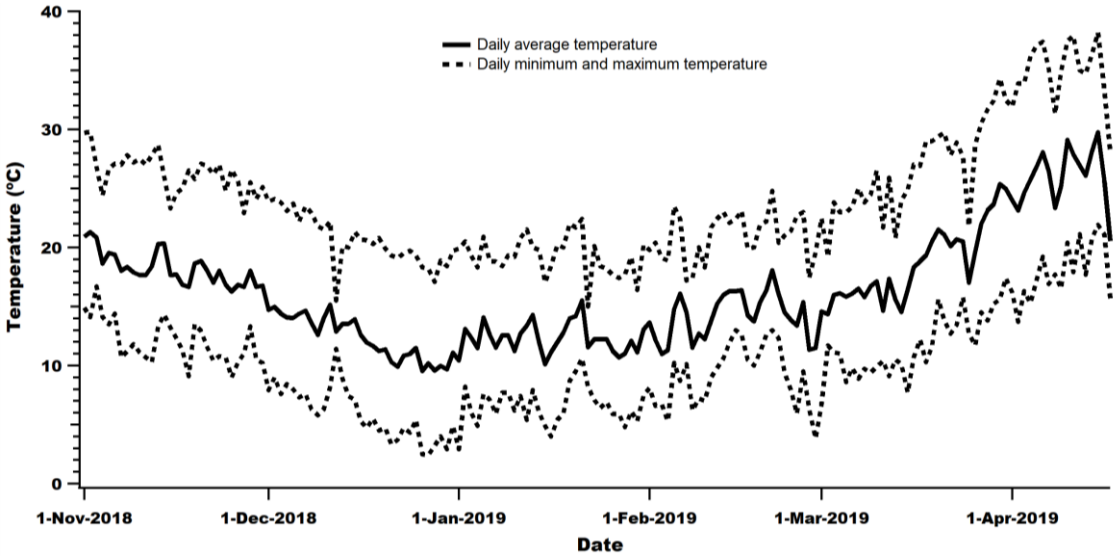

Figure 3: A time series of temperature observed during 2018-19 winter and early summer of 2019, at the Central Atmospheric Chemistry facility, IISER Mohali. The solid line represents the daily average and the dotted lines represent the daily minimum and daily maximum.

Annually the NW-IGP receives rainfall due to western disturbances during February and March (figure 5). Instantaneous decline in the daily average and daily maximum temperatures during the same period can be explained by rain events.

4.1.2 Photosynthetically active radiation (PAR)

Photosynthesis is driven by PAR. Therefore variation in PAR directly impacts photosynthesis, which is important for growth and development in all plants. Figure 4 shows a time series plot of PAR recorded during growing season of 2018-19.

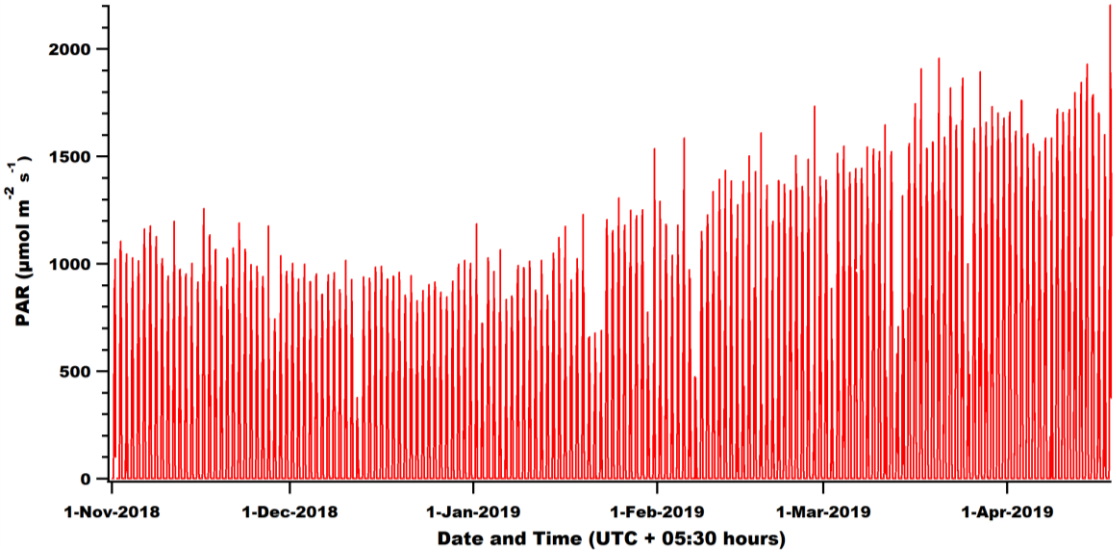

Figure 4: A time series of PAR observed at the Central Atmospheric Chemistry Facility, IISER Mohali, Punjab, India, during 2018-19 winter and early summer of 2019

A maximum PAR of 2240.6 µmol $m^{-2}s^{-1}$ was recorded at 11:13 hours on 17th April 2019. Trends in PAR are similar to that of temperature, where the daily average and daily maximum PAR are lower in the winter months and gradually increase starting from summer (figure 5).

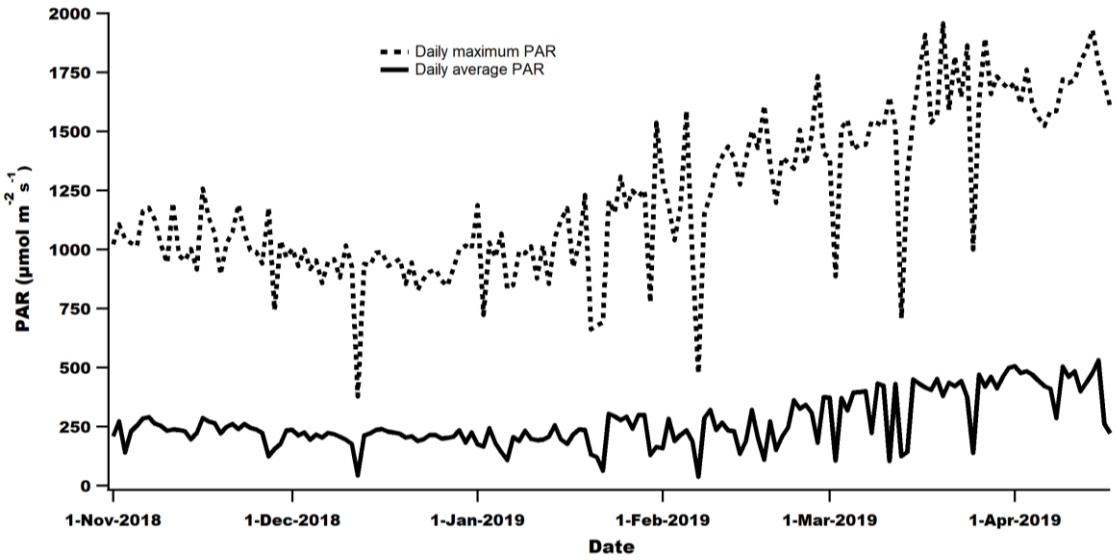

Figure 5: A time series of PAR observed during 2018-19 winter and early summer of 2019 at the Central Atmospheric Chemistry facility, IISER Mohali. The solid line represents the daily average and the dotted line represents the daily maximum.

PAR is directly affected by clouds and rain, which scatter sun's radiation, reducing the amount of radiation reaching the Earth's surface. During winter, there is frequent formation of fog, which also scatters sun's radiation. Therefore events of instantaneous

decrease in PAR values measured can be explained by foggy weather during winter and overcast sky or rainfall during summer.

4.1.3 Rainfall

Although crops cultivated on irrigated farmlands do not depend on rains for water, torrential rains can damage crops. Figure 6 shows a month wise distribution of number of days with rainfall and total monthly rainfall. In total there were 21 days with rainfall, with cumulative growing season rainfall being 173.5mm. A maximum rainfall of 24.5mm was recorded on 14th March 2019. Rainfall in February and March 2019, together account for more than 75% of the total rainfall recorded during the growing season. This is consistent with frequent instantaneous reductions in temperature and PAR values observed during the same period.

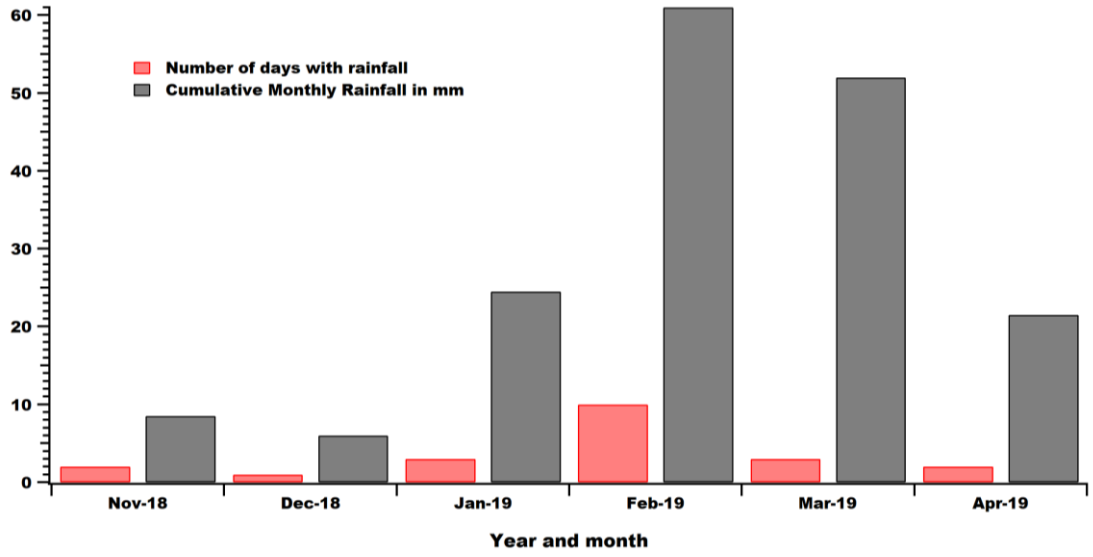

Figure 6: A bar graph showing number of days with rainfall and cumulative monthly rainfall, observed during the winter wheat growing season of 2018-19 at the Central Atmospheric chemistry facility, IISER Mohali.

Torrential rain during harvest can affect the quality of crops and also damage the crops, reducing the yield. Rain during flowering can also negatively affect yield and reduce the number of grains in a head. Winter wheat sown between November and December is expected to reach maturity in April. From the above graph, it can be observed that rainfall in April only amounts to around 12% (21.5 mm) of total growing season rainfall. Therefore rain has negligible impact on the quality and quantity of crops, in this study.

4.1.4 Vapour Pressure Deficit (VPD)

Vapour pressure deficit is the difference between saturation vapour pressure and observed vapour pressure. It is a function of temperature and one of the important meteorological parameters that controls the opening and closing of stomata.

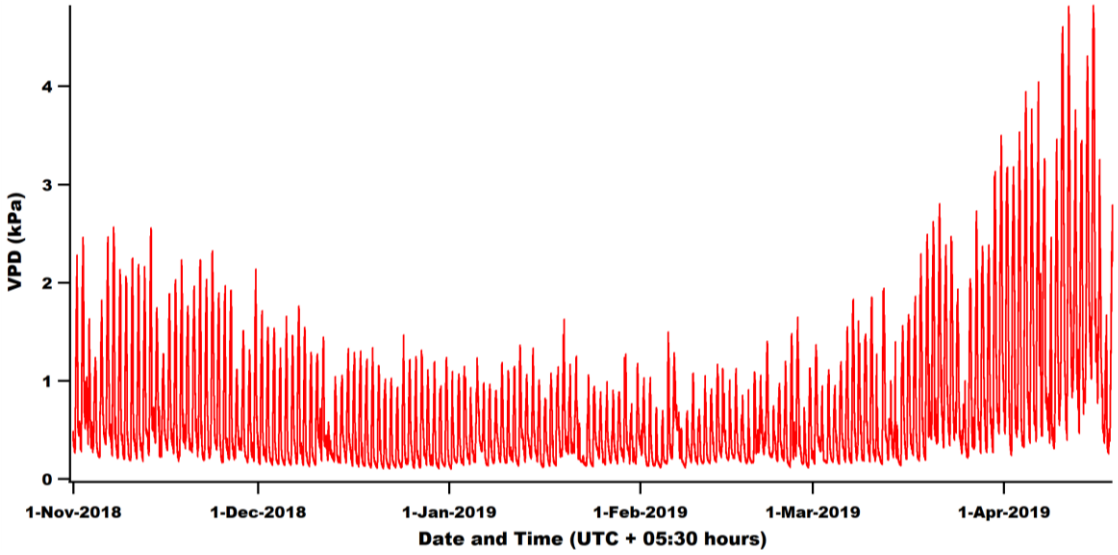

Figure 7: A time series plot of VPD observed during the winter wheat growing season of 2018-19 at the Central Atmospheric Chemistry facility, IISER Mohali.

Figure 7 shows a time series of VPD observed during the growing season and figure 8 shows the daily average, daily minimum and daily maximum VPD.

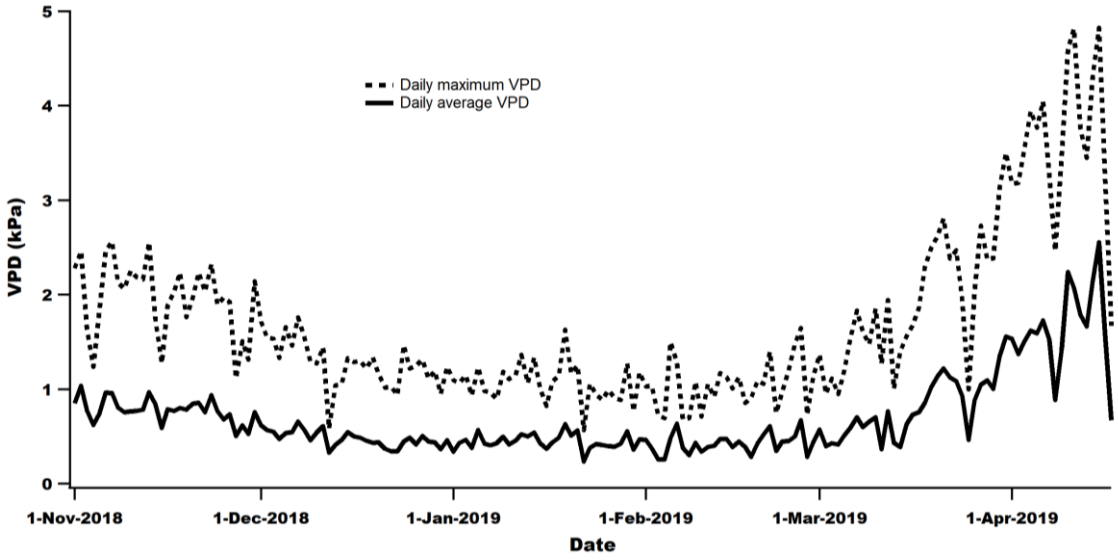

Figure 8: A time series plot of VDP, observed during winter wheat growing season of 2018-19 at the Central Analytical Chemistry facility, IISER Mohali. The solid curve represents the daily average and the dotted curve represents the daily minimum and daily maximum

Since VPD is a function of temperature, trends in VPD are similar to that in temperature; it is the dependence of VPD on temperature is exponential (figure 7). Stomata remain open when VPD is low, allowing for passage of gases into and out of leaves, thereby impacting photosynthesis. However, high VDP occurs at high temperatures, which is frequently observed during the summer months, as observed in figure 7. This poses a risk of increased evapotranspiration, which can damage the crop if water stress exits. In this study, soil moisture was maintained at healthy levels throughout. A maximum VPD of 4.82 kPa was observed at 13:37 hours on 15th April 2019. Instantaneous dip observed in VPD values is due to rain.

4.1.5 Wind speed

A time series of daily average wind speeds during the winter wheat growing season of 2018-19 observed at the Central Atmospheric chemistry facility, IISER Mohali, is shown in figure 9. Hot air rises up, creating low pressure regions. Air parcels then flow from high pressure region to low pressure region. Since average temperatures are higher during summer, winds are stronger during dry conditions.

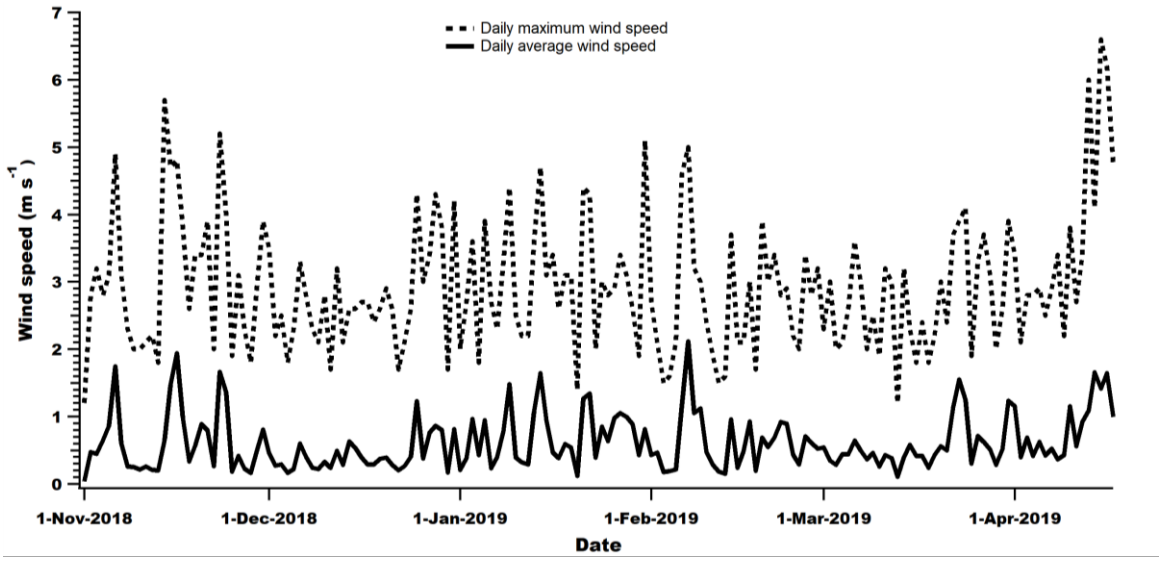

Figure 9: A time series of daily average wind speeds during the winter wheat growing season of 2018-19 observed at the Central Atmospheric chemistry facility, IISER Mohali

At high speeds, winds can uproot plants or cause physical damage to them. On the other hand, high wind speeds are responsible for large scale transport of atmospheric gases. Aphalo et al, (1993) has shown that wind alters the leaf boundary layer thickness, changing the mole fraction of CO_2 and water vapour at the boundary layer. Stomatal

conductance is sensitive to these changes. Therefore wind speed indirectly impacts stomatal conductance.

4.1.6 Tropospheric Ozone

A time series of daily average O_3 concentrations, along with daily maximum and M7 concentrations is shown in figure 10. O_3 is formed by NO_x and VOC (Volatile organic compounds) precursors only in the presence of sunlight. Hence the average concentration of O_3 is expected to be the maximum in the summer months - where high temperature and PAR, and low relative humidity (RH) favour ozone formation - and low tropospheric O_3 concentrations are expected in the winter months. However, in the NW-IGP, paddy residue burning that happens annually after the harvest of kharif crops, between October and December, contributes to enhanced tropospheric O_3 concentrations in this period (Kumar et al., 2016). This is consistent with the concentrations observed during November and December 2018, where the M7 and daily maximum values can be seen exceeding those in the summer months (figure 10). A maximum tropospheric O_3 concentration of 132.43 ppb was observed on 8th November 2018 and on 6th April 2019, a maximum M7 concentration of 85.34ppb was observed. The precursors of tropospheric O_3 are washed away by rain, which explains the instantaneous dip in O_3 concentrations observed.

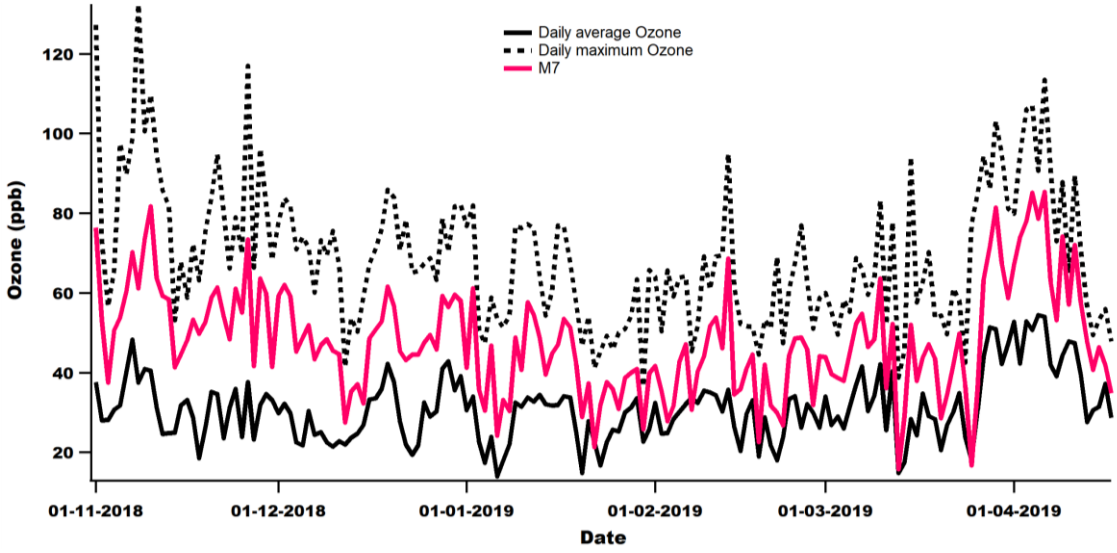

Figure 10: A time series of tropospheric ozone concentrations observed at the Central Atmospheric Chemistry facility, IISER Mohali, during the winter wheat growing season of 2018-19. Solid black line represents the daily average, solid pink line represents M7 and the dotted line represents the daily maximum concentrations.

4.2 Wheat phenology results

The wheat seeds of an Indian winter wheat cultivar popular in the NW-IGP, sown on 3 different dates – 1st November, 15th November and 1st December 2018 – were harvested on 10th April, 14th April and 18th April 2019, respectively. The phenology data of different growth stages – flag leaf, heading and anthesis - from different plots noted down as fraction emerged (fraction of plants reaching that particular stage) plotted against DAS, is shown in figure 11. The data was fit to a sigmoid function, since each stage of plant growth follows a sigmoid growth curve. For a given plot and given growth stage, X_{half} parameter calculated from the fit gives the amount of time taken for 50% of all plants on that plot to reach that particular stage. The value of X_{half} represents the whole set of plants, for a given plot. The difference in time taken by different plots to reach different growth stages is evident from figure 11, where 3 plots in the top row are for plot 1, those in the middle and the last row are for plots 2 and 3 respectively.

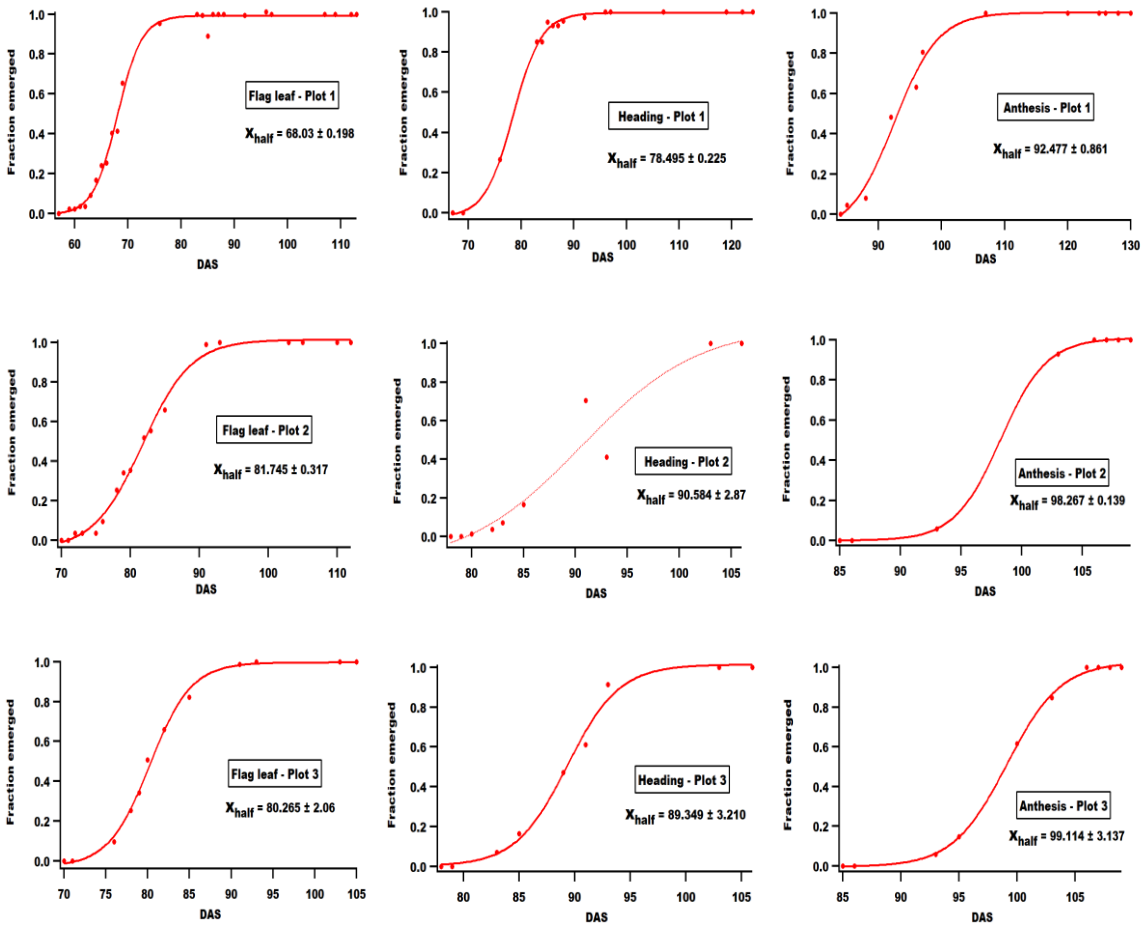

Figure 11: Phenology data of different growth stages plotted against DAS. The data is fit to a sigmoid curve. Top row is for plot 1, middle row for plot 2 and last row for plot 3.

The duration for PBW550 in different plots to reach flag leaf, heading, anthesis and maturity stages is detailed in Table 2. The number of days for wheat to reach maturity was 160, 149 and 138 in plots 1, 2 and 3 respectively. While plot 1 reached flag leaf stage after 68 days, plots 2 and 3 needed more than 80 days for the same. Although the number of days between flag leaf and heading, and heading and anthesis stages did not differ much, the grain filling duration, in other words, difference between the number of days between anthesis and maturity, differed significantly with 67.5, 51.7 and 39 days for plots 1, 2 and 3 respectively. The shortening of grain filling duration for plots 2 and 3 relative to plot 1, is examined in the upcoming sections

Table 2: Time in days after sowing (DAS) and growing degree days (GDD) for different stages of different plots

Plot Number	**Flag leaf** (DAS)	**Flag leaf** (GDD in ^{o}C-days)	**Heading** (DAS)	**Heading** (GDD in ^{o}C-days)	**Anthesis** (DAS)	**Anthesis** (GDD in ^{o}C-days)	**Maturity** (DAS)	**Maturity** (GDD in ^{o}C-days)
Plot 1	68.0 ± 0.2	1015 ± 3	78.5 ± 0.2	1136 ± 3	92.5 ± 0.8	1310 ± 11	160	2723
Plot 2	81.7 ± 0.3	1072 ± 4	90 ± 2	1198 ± 27	98.3 ± 0.1	1325 ± 2	150	2437
Plot 3	80 ± 2	1067 ± 26	89 ± 3	1161 ±39	99 ± 3	1306 ± 39	138	2162

4.2.1 Temperature and wheat phenology

Temperature is the major driver of wheat growth and development. In the absence of water and nutrient stress, as in the case of this study, phenology is a function of temperature alone. Leaf area changes with growth stages, where it increases up to anthesis and starts reducing post-anthesis. Hence it can be used as a proxy to understand wheat phenology. Temperature has direct impacts on leaf area growth; Asseng et.al (2011) reported that the optimum daily mean temperature range for leaf area growth in wheat is between 11^{o}C and 24^{o}C, and that daily mean temperatures out of this range would reduce the rate of leaf growth. The study further identified the daily maximum temperature above which leaf senescence hastens as 34^{o}C. Therefore exposure to

temperatures above 34^{o}C affects wheat plants by reducing the leaf area available for photosynthesis, thereby reducing the yield.

Plots 1, 2 and 3 were sown and harvested on different dates, which made the growing conditions, particularly temperature, different for same growth phases of different plots. A time series plot of daily average temperature overlaid on a background showing time taken in days after sowing to reach different growth stages is shown in figure 12. The average daily temperatures during the vegetative growth stages (Emergence and Flag leaf) are important since most of the leaf growth and development takes place during these stages. Although for most duration through the emergence and flag leaf stage the daily average temperature was within the optimum range for all plots, on some days the temperature dropped below the minimum threshold of 11^{o}C (figure 12).

While plot 1 experienced 10 days with daily average temperature less than 11^{o}C, plots 2 and 3 experience 13 days each. This could have slowed down the process of leaf area growth. However, the effect of heat stress is greater on leaf area. Clearly, all plots experienced heat stress events during grain filling (figure 12). Plots 1, 2 and 3 experienced 6, 10 and 12 days of heat stress respectively. But what is more important here is the timing of heat stress experienced by different plots; (i) for plot 1, the first heat stress event occurred 149 days after sowing, or in other words, 57 days after anthesis, (ii) for plot 2, the first heat stress event occurred 37 days after anthesis (110 DAS) and (iii) for plot 3, the first heat stress event occurred 20 days after anthesis. Since leaf area reduces post-anthesis, hastening of leaf senescence by heat stress adds to reduction is leaf area available for photosynthesis. Early heat stress events experienced by plots 2 and 3 resulted in shortening of grain filling duration. To substantiate the fact that the reduction in leaf area was accelerated in plots 2 and 3, we use stomatal conductance measurements. The related results are detailed in the upcoming sections.

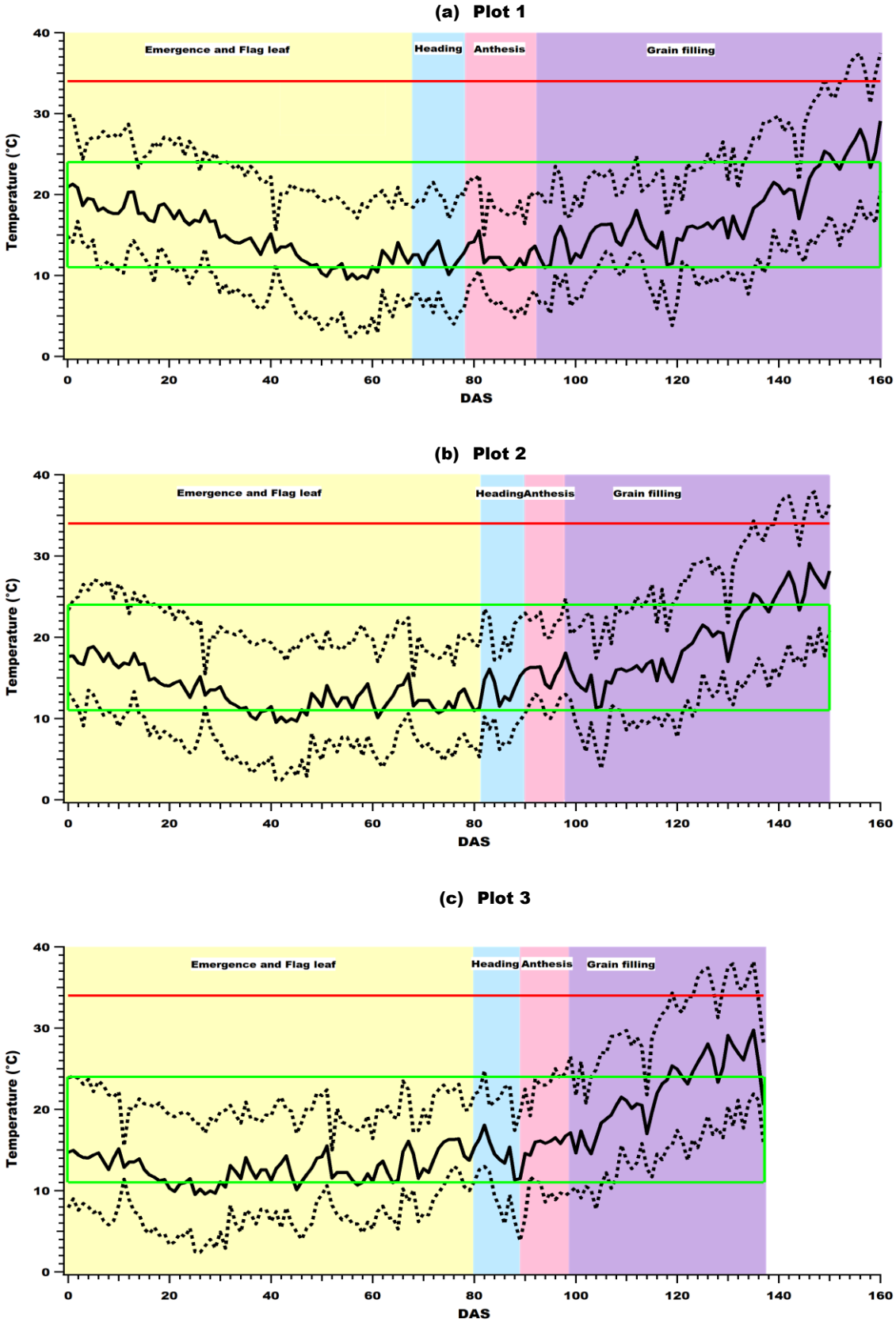

Figure 12: A time series plot of temperature overlaid on a background showing shaded regions corresponding to days after sowing (DAS) taken to complete different growth stages for (a) Plot 1 (b) Plot and (c) Plot 3. The solid black line represents the daily average temperature and dotted black lines represent the daily minimum and daily maximum temperatures. The box outlined in green is the temperature range optimum for leaf growth and the solid red line represents the temperature threshold of 34^{o}C, beyond which leaf senescence hastens.

4.2.2 Ozone and wheat phenology

Tropospheric O_3 is also known to accelerate leaf senescence in plants. Table 3 lists the average O_3 concentrations in M7 and summed AOT40 concentrations in ppb, measured between different growth stages for different plots.

Table 3: Concentrations of O_3 in ppb, observed between successive growth stages for plots 1, 2 and 3, expressed using M7 and AOT40 metrics

Growth stage	**Emergence and flag leaf**		**Heading**		**Anthesis**		**Grain filling**	
Metric	**M7**	**AOT40**	**M7**	**AOT40**	**M7**	**AOT40**	**M7**	**AOT40**
Plot 1	50.8	9884.2	48.6	1340.6	35.3	510.8	46.0	8671.5
Plot 2	45.7	9053.7	45	977.2	33.2	496.0	49.9	8105.9
Plot 3	43.6	7629.5	38.3	553.7	44.5	675.3	51.5	7066.17

The total AOT40 value is the highest for plot 1, which is expected because of longer growth duration, while different plots had different M7 values during different growth stages. However, both M7 and AOT40 are concentration based O_3 metrics, which do not give the stomatal ozone flux. Therefore it is necessary to understand during which growth stage the stomatal conductance peaks and then check the tropospheric O_3 concentration metrics, in order to estimate the stomatal flux of O_3.

4.3 Stomatal conductance measurements

Stomatal conductance gives the flux of water vapour or CO_2 through stomata. The total flux is physically limited by available leaf area and opening of stomata, which are in turn controlled externally by meteorological factors. For a given leaf area, opening of stomata is controlled by temperature, soil moisture, VPD and wind speed. Having known the effect of temperature on leaf area growth, the diel cycle profiles of meteorological parameters shown in figure 13 is important to understand their effect on stomatal conductance, on a given day, with known leaf area.

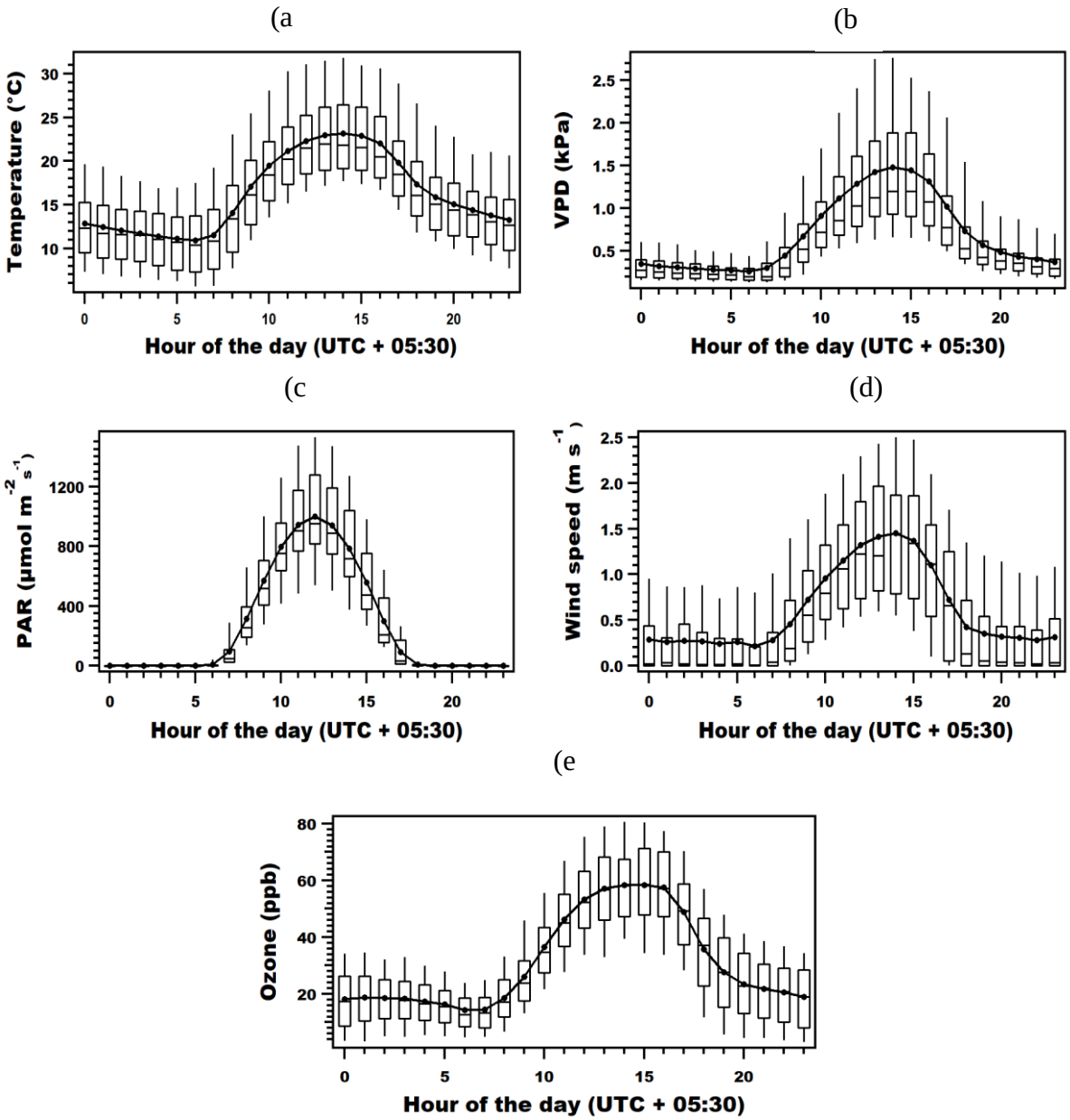

Figure 13: Box and whisker plots showing the diel cycle in (a) Temperature (b) VPD (c) PAR (d) Wind speed and (e) Ozone, observed at the Central Atmospheric Facility, IISER Mohali, during the wheat growing season of 2018-19. All measurements taken during a certain hour of the day during the entire growing season are binned into hours. The lower and upper limit of the box represents 75th and 25th percentile respectively, the horizontal line in the middle of the box represents the median and the dot inside each box represents the average. The Whiskers show the 90th and 10th percentile of the data.

4.3.1. Modelling stomatal flux of O_3 - Environmental response functions for stomatal conductance

The DO_3SE model uses a multiplicative algorithm to calculate the stomatal conductance for ozone, which is explained in the previous chapter. The limiting functions for stomatal conductance used in the model are g_{max}, f_{temp}, f_{light}, f_{VPD} and f_{phen}. All functions were parametrised for PBW550 cultivar, using the measured stomatal conductance data. The variation in the measured stomatal conductance with temperature, PAR and VPD is shown in figure 14. The parameters that were used to fit the maximum curve for each parameter are compared with the values listed in the DO_3SE manual, in table 4.

Table 4: Calculated values of functions limiting ozone stomatal conductance and parameters used for fitting maximum curve, compared with the values listed in the DO_3SE manual.

Function	Fit parameters for maximum curve	Value listed in DO_3SE manual	Value calculated from this study
g_{max}	-	500 mmol O_3 m^{-2} PLA s^{-1}	560 mmol O_3 m^{-2} PLA s^{-1}
f_{temp}	t_{min}	12°C	4°C
	t_{opt}	26°C	25°C
	t_{max}	40°C	37°C
f_{light}	light_a	0.0105	0.004
f_{VPD}	VPD_{max}	1.2 kPa	3.6 kPa
	VPD_{min}	3.2 kPa	4.9 kPa

The conditions when stomatal conductance for ozone reaches maximum for temperature, PAR and VPD can be identified from figures 14(a), 14(b) and 14(c) respectively. The O_3 stomatal conductance peaks at 25°C, and drops down on moving towards either side of the maximum curve. It reaches minimum at 4°C and 37°C. The maximum measure of VPD up to which conductance remains high is 3.6 kPa. Beyond this value stomata begin closing down to avoid excess evapotranspiration and conductance starts reducing, reaching minimum at 4.9 kPa.

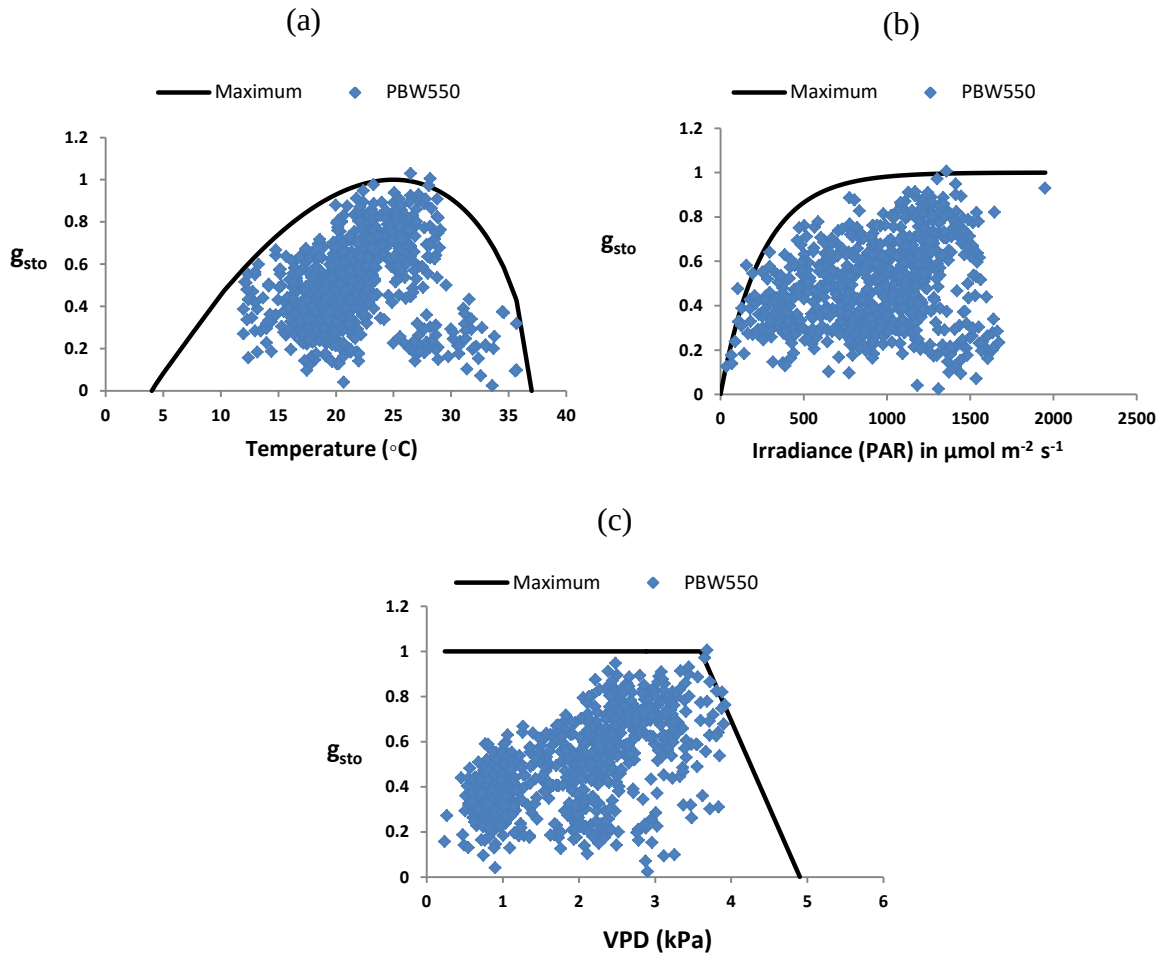

Figure 14: Measured stomatal conductance plotted with (a) Temperature (b) PAR and (c) VPD. The fit parameters listed in table 3 are used for fitting the maximum curves

The phenology function described in the DO_3SE manual only allows making straight lines between one developmental phase and other. It also does not take into account effects of heat stress on phenology, which is important and can cause significant changes. Hence a new phenology function was derived, which accounts for impacts of both, ozone and heat stress, on phenology.

4.4 Applying post-anthesis heat stress to phenology

All plots experienced post-anthesis heat stress (figure 12), which accelerates leaf senescence. Any change in leaf area is associated changes in number of stomata, which changes stomatal conductance; stomatal conductance can therefore be used as a proxy to model leaf area change.

Heat stress applied to post-anthesis stomatal conductance using the heat stress function given by Asseng et.al (2011) is shown in figure 15, along with measured stomatal conductance.

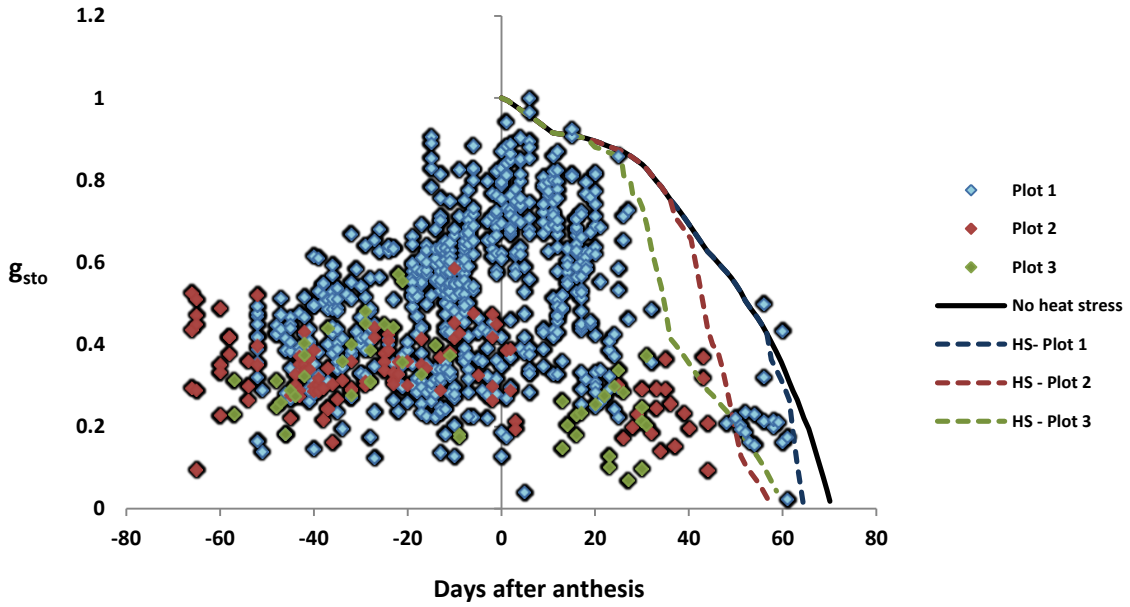

Figure 15: Impact of heat stress on post-anthesis stomatal conductance. Blue, red and green markers are measured stomatal conductance values from plots 1, 2 and 3 repectively. The solid black curve is the modelled behaviour of post-anthesis stomatal conductance, with no heat stress. Blue dotted line shows the modelled behaviour of post-anthesis stomatal conductance for plot 1, with heat stress applied while red and green dotted lines represent the same for plots 2 and 3 respectively.

The zero of the horizontal axis marks the day of anthesis. On comparing the solid black curve with any of the other 3 curves, it is evident that application of heat stress accelerated the reduction in stomatal conductance, although the behaviour of modelled stomatal conductance is different for all plots. This is expected since the timing and number of days of heat stress was different for all plots. An interesting observation is that, although plot 3 experienced post-anthesis heat stress much earlier and for greater number of days compared to plot 2, the modelled behaviour predicts a longer grain filling duration for plot 3. Therefore the timing of heat stress seems to have a stronger influence in predicting the behaviour of stomatal conductance subjected to post-anthesis heat stress. Comparing the modelled and measured stomatal conductance, the model predicts the change in stomatal conductance for plot 1 with good accuracy. However, plots 2 and 3 exhibit behaviours different from the model prediction. The stomatal conductance values in both plots drop to minimum much earlier than the model predicts, with the difference

being greater for plot 3. This is observed because the function used to model the effects of heat stress does not take into account the impacts of tropospheric O_3 on phenology. In the next section we derive one such function which accounts for the impacts of both heat stress and O_3 on stomatal conductance.

From figure 15, we see that stomatal conductance is highest around anthesis. Therefore high O_3 concentrations during anthesis results in increased stomatal flux of O_3, which accelerates leaf senescence. From table 3, we see that the M7 value is highest for plot 3 during anthesis and grain filling. Combined with heat stress, O_3 flux further shortens the grain filling duration for plot 3.

4.5 A new phenology function

The measured stomatal conductance was plotted against days after anthesis and the maximum curve was fit using a function of the following form:

$$f_{phen} = \begin{cases} 1 - a(-DAA), & for\ DAA \leq 0 \\ \dfrac{1}{1 + b * \exp(c * DAA)} & for\ DAA > 0 \end{cases}$$

where DAA is days after anthesis and a, b and c are constants which depend on the cultivar used and sowing date. The maximum fit curve is shown below in figure 16.

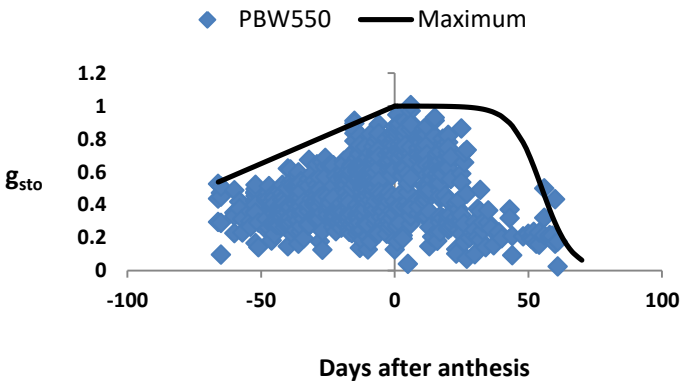

Figure 16: Maximum function for the new phenology function, with a = 0.007, b = 0.0005 and c = 0.18

Chapter 5

Conclusions

Growing season length in wheat is sensitive to heat stress and high stomatal ozone flux. Presence of both these stress factors accelerates leaf senescence, shortening the grain filling duration. Even though winter wheat cultivars suited for late sowing exist, if they are only tolerant to heat stress, significant damage can be caused by ozone flux.

On the modelling front, it is important to incorporate effects of both heat stress and ozone flux, into both, crop simulation models and models such as DO_3SE, which simulate stomatal conductance. In crop simulation models, not accounting for ozone flux leads to over estimation of grain filling duration. The form of the phenology function in DO_3SE model needs to be modified to incorporate heat stress and also to reduce the uncertainty between simulated and observed changes in stomatal conductance changes over the growing period.

Bibliography

Peer reviewed journals

Acevedo, E., Silva, P. and Silva, H., 2002. Wheat growth and physiology. *Bread Wheat, Improvement and Production*, *30*.

Ainsworth, Elizabeth A. 2017. "Understanding and Improving Global Crop Response to Ozone Pollution." *The Plant Journal* 90 (5): 886–97. https://doi.org/10.1111/tpj.13298.

Ainsworth, Elizabeth A., Craig R. Yendrek, Stephen Sitch, William J. Collins, and Lisa D. Emberson. 2012. "The Effects of Tropospheric Ozone on Net Primary Productivity and Implications for Climate Change." *Annual Review of Plant Biology* 63 (1): 637–61. https://doi.org/10.1146/annurev-arplant-042110-103829.

Asseng, S., F. Ewert, P. Martre, R. P. Rötter, D. B. Lobell, D. Cammarano, B. A. Kimball, et al. 2015. "Rising Temperatures Reduce Global Wheat Production." *Nature Climate Change* 5 (2): 143–47. https://doi.org/10.1038/nclimate2470.

Asseng, S., F. Ewert, C. Rosenzweig, J. W. Jones, J. L. Hatfield, A. C. Ruane, K. J. Boote, et al. 2013. "Uncertainty in Simulating Wheat Yields under Climate Change." *Nature Climate Change* 3 (9): 827–32. https://doi.org/10.1038/nclimate1916.

Asseng, Senthold, Ian Foster, and Neil C. Turner. 2011. "The Impact of Temperature Variability on Wheat Yields." *Global Change Biology* 17 (2): 997–1012. https://doi.org/10.1111/j.1365-2486.2010.02262.x.

Avnery, Shiri, Denise L. Mauzerall, Junfeng Liu, and Larry W. Horowitz. 2011. "Global Crop Yield Reductions Due to Surface Ozone Exposure: 1. Year 2000 Crop Production Losses and Economic Damage." *Atmospheric Environment* 45 (13): 2284–96. https://doi.org/10.1016/j.atmosenv.2010.11.045.

Barlow, K.M., B.P. Christy, G.J. O'Leary, P.A. Riffkin, and J.G. Nuttall. 2015. "Simulating the Impact of Extreme Heat and Frost Events on Wheat Crop Production: A Review." *Field Crops Research* 171 (February): 109–19. https://doi.org/10.1016/j.fcr.2014.11.010.

BROOKING, I.R., 1996. Temperature response of vernalization in wheat: a developmental analysis. *Annals of Botany*, *78*(4), pp.507-512.

Cao, W. and Moss, D.N., 1989. Temperature effect on leaf emergence and phyllochron in wheat and barley. *Crop Science*, *29*(4), pp.1018-1021.

Chhuneja, Parveen, Jaskaran Kaur Arora, Pawandeep Kaur, Satinder Kaur, and Kuldeep Singh. 2015. "Characterization of Wild Emmer Wheat Triticum Dicoccoides Germplasm for Vernalization Alleles." *Journal of Plant Biochemistry and Biotechnology* 24 (2): 249–53. https://doi.org/10.1007/s13562-014-0281-7.

CLRTAP, 2015. Mapping Critical Levels for Vegetation, Chapter III of Manual on methodologies and criteria for modelling and mapping critical loads and levels and air pollution effects, risks and trends. https://icpvegetation.ceh.ac.uk/chapter-3-mapping-critical-levels-vegetation

Danielsson, H., Karlsson, G.P., Karlsson, P.E. and Pleijel, H.H., 2003. Ozone uptake modelling and flux-response relationships—an assessment of ozone-induced yield loss in spring wheat. *Atmospheric Environment*, *37*(4), pp.475-485.

Debaje, S. B. 2014. "Estimated Crop Yield Losses Due to Surface Ozone Exposure and Economic Damage in India." *Environmental Science and Pollution Research* 21 (12): 7329–38. https://doi.org/10.1007/s11356-014-2657-6.

Dubey, Rachana, Himanshu Pathak, Bidisha Chakrabarti, Shivdhar Singh, Dipak Kumar Gupta, and R.C. Harit. 2020. “Impact of Terminal Heat Stress on Wheat Yield in India and Options for Adaptation.” *Agricultural Systems* 181 (May): 102826. https://doi.org/10.1016/j.agsy.2020.102826.

El Wazziki, H., El Yousfi, B. and Serghat, S., 2015. Contributions of three upper leaves of wheat, either healthy or inoculated by'Bipolaris sorokiniana', to yield and yield components. *Australian Journal of Crop Science*, *9*(7), p.629.

Emberson, L.D., Ashmore, M.R., Cambridge, H.M., Simpson, D. and Tuovinen, J.P., 2000. Modelling stomatal ozone flux across Europe. *Environmental Pollution*, *109*(3), pp.403-413.

Hall, A. E. 2001. *Crop Responses to Environment*. Boca Raton: CRC Press.

Iqbal, Muhammad, Naveed Iqbal Raja, Farhat Yasmeen, Mubashir Hussain, Muhammad Ejaz, and Muhammad Ali Shah. 2017. “Impacts of Heat Stress on Wheat: A Critical Review.” *Advances in Crop Science and Technology* 5 (1). https://doi.org/10.4172/2329-8863.1000251.

Jarvis, P.G., 1976. The interpretation of the variations in leaf water potential and stomatal conductance found in canopies in the field. *Philosophical Transactions of the Royal Society of London. B, Biological Sciences*, *273*(927), pp.593-610.

Joshi, S. K., S. N. Sharma, D. L. Singhania, and R. S. Sain. 2003. “Genetic Analysis of Yield and Its Component Traits in Spring Wheat.” *Acta Agronomica Hungarica* 51 (2): 139–47. https://doi.org/10.1556/AAgr.51.2003.2.1.

Jones, J.W., Hoogenboom, G., Porter, C.H., Boote, K.J., Batchelor, W.D., Hunt, L.A., Wilkens, P.W., Singh, U., Gijsman, A.J. and Ritchie, J.T., 2003. The DSSAT cropping system model. *European journal of agronomy*, *18*(3-4), pp.235-265.

Kirby, E.J.M., 2002. Botany of the wheat plant. *Bread Wheat. Improvement and Production. Food and Agriculture Organization of the United Nation. Rome*, pp.19-37.

Kumar, S., Sharma, V., Chaudhary, S., Tyagi, A., Mishra, P., Priyadarshini, A. and Singh, A., 2012. Genetics of flowering time in bread wheat Triticum aestivum: complementary interaction between vernalization-insensitive and photoperiod-insensitive mutations imparts very early flowering habit to spring wheat. *Journal of genetics*, *91*(1), pp.33-47.

Kumar, V., Sarkar, C. and Sinha, V., 2016. Influence of post-harvest crop residue fires on surface ozone mixing ratios in the NW IGP analyzed using 2 years of continuous in situ trace gas measurements. *Journal of Geophysical Research: Atmospheres*, *121*(7), pp.3619-3633.

Liu, Bing, Senthold Asseng, Leilei Liu, Liang Tang, Weixing Cao, and Yan Zhu. 2016. “Testing the Responses of Four Wheat Crop Models to Heat Stress at Anthesis and Grain Filling.” *Global Change Biology* 22 (5): 1890–1903. https://doi.org/10.1111/gcb.13212.

Lobell, David B., Adam Sibley, and J. Ivan Ortiz-Monasterio. 2012a. “Extreme Heat Effects on Wheat Senescence in India.” *Nature Climate Change* 2 (3): 186–89. https://doi.org/10.1038/nclimate1356.

———. 2012b. “Extreme Heat Effects on Wheat Senescence in India.” *Nature Climate Change* 2 (3): 186–89. https://doi.org/10.1038/nclimate1356.

Martre, Pierre, Daniel Wallach, Senthold Asseng, Frank Ewert, James W. Jones, Reimund P. Rötter, Kenneth J. Boote, et al. 2015. “Multimodel Ensembles of Wheat Growth: Many Models Are Better than One.” *Global Change Biology* 21 (2): 911–25. https://doi.org/10.1111/gcb.12768.

Mills, G., A. Buse, B. Gimeno, V. Bermejo, M. Holland, L. Emberson, and H. Pleijel. 2007. “A Synthesis of AOT40-Based Response Functions and Critical Levels of Ozone for Agricultural and Horticultural Crops.” *Atmospheric Environment* 41 (12): 2630–43. https://doi.org/10.1016/j.atmosenv.2006.11.016.

Mills, Gina, Håkan Pleijel, Sabine Braun, Patrick Büker, Victoria Bermejo, Esperanza Calvo, Helena Danielsson, et al. 2011a. “New Stomatal Flux-Based Critical Levels for Ozone Effects on Vegetation.” *Atmospheric Environment* 45 (28): 5064–68. https://doi.org/10.1016/j.atmosenv.2011.06.009.

———. 2011b. “New Stomatal Flux-Based Critical Levels for Ozone Effects on Vegetation.” *Atmospheric Environment* 45 (28): 5064–68. https://doi.org/10.1016/j.atmosenv.2011.06.009.

Mills, Gina, Katrina Sharps, David Simpson, Håkan Pleijel, Malin Broberg, Johan Uddling, Fernando Jaramillo, et al. 2018a. “Ozone Pollution Will Compromise Efforts to Increase Global Wheat Production.” *Global Change Biology* 24 (8): 3560–74. https://doi.org/10.1111/gcb.14157.

———. 2018b. “Ozone Pollution Will Compromise Efforts to Increase Global Wheat Production.” *Global Change Biology* 24 (8): 3560–74. https://doi.org/10.1111/gcb.14157.

Ortiz-Monasterio R., J.I., S.S. Dhillon, and R.A. Fischer. 1994. “Date of Sowing Effects on Grain Yield and Yield Components of Irrigated Spring Wheat Cultivars and Relationships with Radiation and Temperature in Ludhiana, India.” *Field Crops Research* 37 (3): 169–84. https://doi.org/10.1016/0378-4290(94)90096-5.

Pleijel, H., Danielsson, H., Emberson, L., Ashmore, M.R. and Mills, G., 2007. Ozone risk assessment for agricultural crops in Europe: Further development of stomatal flux and flux–response relationships for European wheat and potato. *Atmospheric Environment*, *41*(14), pp.3022-3040.

Porter, J.R. and Gawith, M., 1999. Temperatures and the growth and development of wheat: a review. *European journal of agronomy*, *10*(1), pp.23-36.

Rötter, Reimund P., Timothy R. Carter, Jørgen E. Olesen, and John R. Porter. 2011. “Crop–Climate Models Need an Overhaul.” *Nature Climate Change* 1 (4): 175–77. https://doi.org/10.1038/nclimate1152.

Sinha, B., Sangwan, K.S., Maurya, Y., Kumar, V., Sarkar, C., Chandra, B.P. and Sinha, V., 2015. Assessment of crop yield losses in Punjab and Haryana using two years of continuous in-situ ozone measurements. *Atmospheric Chemistry & Physics Discussions*, *15*(2).

Zhao, Hui, Tingbo Dai, Qi Jing, Dong Jiang, and Weixing Cao. 2007. “Leaf Senescence and Grain Filling Affected by Post-Anthesis High Temperatures in Two Different Wheat Cultivars.” *Plant Growth Regulation* 51 (2): 149–58. https://doi.org/10.1007/s10725-006-9157-8.

Zheng, B., Chenu, K., Doherty, A. and Chapman, S., 2014. The APSIM-wheat module (7.5 R3008). *Agricultural Production Systems Simulator (APSIM) Initiative*. https://www.apsim.info/wp-content/uploads/2019/09/WheatDocumentation.pdf